Electronic Supplementary Material (ESI) for Journal of Materials Chemistry A.
This journal is © The Royal Society of Chemistry 2022

Supporting Information

Achieving a High Selectivity for Nitrate Electrochemical Reduction to Ammonia over MOF-Supported Ru_xO_y Clusters

Jiangzhou Qin,[a] Kun Wu,[a] Liuzhou Chen,[a] Xintao Wang,[a] Quanlin Zhao,[a] Baojun Liu*[b] and Zhengfang Ye*[a]

a. *Department of Environmental Engineering, Peking University, The Key Laboratory of Water and Sediment Sciences, Ministry of Education, Beijing, 100871, China.*
E-mail: zhengfangye@163.com

b. *College of Resource and Environmental Engineering, Guizhou University, Guizhou Karst Environmental Ecosystems Observation and Research Station, Key Laboratory of Karst Georesources and Environment, Ministry of Education, Guiyang, 550025, China.*
E-mail: jbliu@gzu.edu.cn

1. Material Characterization:

The morphology of various electrodes was observed by field-emission scanning electron microscopy (FESEM, ZEISS Merlin, ΣIGMA+X-Max20) at an acceleration voltage of 10.0 kV and transmission electron microscopy (TEM, JEM-2100F electron microscope, JEOL, Japan) at an acceleration voltage of 200 kV. X-ray diffraction (XRD, Empyrean, Netherlands) was measured with a power X-ray diffractometer (Smartlab 9, Rigaku). X-ray photoelectron spectra (XPS) were collected by a Thermo ESCALAB 250xi X-ray photoelectron spectrometer with Al Kα X-ray (1486.6 eV), as the excitation source. 1H NMR (Bruker, AVANCE III, 600 MHz) spectra were obtained using $^{15}NO_3^-$. The X-ray absorption near edge structures (XANES) and Extended x-ray absorption fine structure (EXAFS) were performed at the Super Photon ring-8 (SPring-8) of Harima Science Garden City, Hyogo in Japan. Ring: 8.0 GeV (996 mA-99.5 mA).

2. Product Quantification:

The UV-Vis spectrophotometer was used to detect the ion concentration of pre- and post-test electrolytes after dilution to appropriate concentration to match the range of calibration curves. The specific detection methods are as follow:

2.1 The detection of NH_4^+-N yields:

The NH_4^+-N yields were determined by a colorimetric method using the Nessler reagent, as reported elsewhere.

Preparation of Nessler's reagent: First, 16.0 g of sodium hydroxide (NaOH) was dissolved in 50 mL ultrapure water. Then, 7.0 g of potassium iodide (KI) and 10.0 g of

mercury iodide (HgI_2) were also dissolved in 20 mL ultrapure water. The above solution was gradually added to the 50 mL sodium hydroxide solution under strong agitation. Finally, the mixture was diluted to 100 mL with ultrapure water.

The preparation of sodium potassium tartrate solution (ρ = 500 $g \cdot L^{-1}$): First, 50.0 g of sodium potassium tartrate ($KNaC_4H_6O_6 \cdot 4H_2O$) was dissolved in 100 mL ultrapure water, and then boiled to remove the residual ammonium. Finally, the solution was diluted to 100 mL after cooling down to ambient temperature.

In details, 1.0 mL electrolyte was taken out from the electrolytic cell and diluted to 10 mL up to the detection range. 0.2 mL of sodium potassium tartrate solution and 0.2 mL of Nessler's reagent were added onto the above solution. After shaking and standing for 20 minutes, the absorbance was tested by UV-Vis spectrophotometry at a wavelength of 420 nm. The concentration–absorbance curve was calibrated by using standard NH_4Cl solutions at a series of concentrations, and the fitting curve is y = 0.1645x + 0.0075 (R^2 = 0.995)

2.2 The detection of NO_3^--N yields:

Firstly, 0.2 mL electrolyte was taken out from the electrolytic cell and diluted to 10 mL to detection range. Then, 0.2 mL 1 M HCl and 0.06 mL 0.8 wt % sulfamic acid solution were added into the aforementioned solution. After 15 minutes, the absorbance was detected by UV-Vis spectrophotometry at a wavelength of 220 nm and 275 nm. The final absorbance of NO_3^--N was calculated based on the following equation: $A=A_{220nm} -2A_{275nm}$. The calibration curve can be obtained through different concentrations of

$NaNO_3$ solutions and the corresponding absorbance (y = 0.2256x + 0.0009, R^2 = 0.9998).

2.3 The detection of NO_2^--N yields:

The color developer was configured as follows: 20 g of p-aminobenzenesulfonamide was added to a mixed solution (250 mL water and 50 mL phosphoric acid), and then 1 g of N-(1-naphthyl)-ethylenediamine dihydrochloride was dissolved in the above solution. Finally, the above solution was transferred to a 500 mL volumetric flask and diluted to the mark.

Specifically, 0.2 mL electrolyte was taken out from the electrolytic cell and diluted to 10 mL to detection range. Next, 0.1 mL color reagent was added into the aforementioned 10 mL solution. After shaking and standing for 20 minutes, the absorbance was subjected to UV-Vis spectrophotometry at a wavelength of 540 nm. The calibration curve can be obtained through different concentrations of $NaNO_2$ solutions and the corresponding absorbance (y = 3.2238x - 0.006, R^2 = 0.9994).

3. Calculation of the yield, selectivity, and Faradaic efficiency.

The concentrations of NH_4^+-N was calculated based on the following equation:

$$NH_4^+\text{-N yield rate} = [c(NH_4^+\text{-N}) \times V] / (t \times m_{cat.})$$

The selectivity of NH_4^+ in the product was calculated based on the following equation:

$$NH_4^+ \text{ selectivity} = c(NH_4^+\text{-N}) / c(NO_3^-\text{-N}) \times 100\%$$

The Faradaic efficiency of NH_4^+ was calculated based on the following equation:

$$\text{Faradaic efficiency} = [8F \times c(NH_4^+\text{-N}) \times V] / [M(NH_4^+\text{-N}) \times Q]$$

where $c(NH_4^+\text{-N})$ was the ammonia concentration, V was the electrolyte volume (120

mL), t was the reaction time (1 h), and $m_{cat.}$ was the mass of the electrocatalyst pipetted onto the carbon paper, F was the Faradaic constant (96485 C mol^{-1}), Q was the total charge passing the electrode.

4. Isotope Labeling Experiments:

$Na^{15}NO_3$ (isotopic abundance: 99 atom%, chemical purity ≥ 98.5%) was used as the feeding N-source to perform the isotopic labeling nitrate reduction experiments to clarify the source of ammonia. After electro-reduction reaction, electrolyte with obtained $^{15}NH_4^+$-^{15}N was taken out and the pH value was adjusted to 2 using 1 M HCl. To further quantifying the concentration of NH_4^+, a series of $^{15}NH_4^+$-^{15}N solutions ($^{15}NH_4Cl$) with known concentration (5, 10, 15, 30, 50 mg/L $^{15}NH_4^+$-^{15}N) were prepared to create the calibration curve. Then, 0.9 mL of the resultant solution was thoroughly mixed with 0.1 mL D_2O for the ^1H nuclear magnetic resonance (NMR) measurement on a Bruker Avance III 600 NMR spectrometer. Similarly, $^{14}NH_4^+$ experiment was also operated in the same way. The calibration curve was obtained through different concentrations of $^{15}NH_4Cl$ solutions and the corresponding absorbance ($y = 51.155x + 262.58$, $R^2 = 0.9991$)

5. FTIR characterization:

In situ FTIR was performed on an IRTracer-100 spectrometer. The electrochemical test was conducted in a custom-made three-electrode electrochemical single cell. A Pt plate and a saturated Ag/AgCl were used as the counter and reference electrodes, respectively. The catalyst electrode was tightly pressed against the window. Firstly, the background value was collected in the presence of RuNi-MOF, H_2O, $NaSO_4$ and

$NaNO_3$. The FTIR spectra were recorded by varying with time during chronoamperometry at -1.6 V vs Ag/AgCl. Finally, the spectra were obtained by subtracting the background from the spectra of samples.

6. *Theoretical calculations:*

The free energy profiles of NO_3^- to NH_3 on Ru nanoparticle were investigated by the Vienna Ab-initio Simulation Package (VASP) with the revised Perdew-Burke-Ernzerh functional of (RPBE) of the generalized gradient approximation (GGA). The interaction between ionic core and valence electrons was calculated by the PAW pseudo-potential. The Ru nanoparticle was simulated by 66 Ru atoms. In the geometry optimization, the energy cutoff of plane-wave basis of 400 eV and energy convergence threshold of 1.0×10^{-5} eV were used. After geometry optimization, the charge density difference mappings between NH_3 and Ru sites were calculated with the Monkhorst-Pack k-point mesh of $2 \times 2 \times 1$. The wider points grid, larger energy cutoff , and higher energy convergence threshold had been examined, which showed the little influence on the electronic calculations. The reported standard hydrogen electrode (SHE) model was used in the calculations of Gibbs free energy changes (ΔG) of all reaction steps. The chemical potential of a proton-electron pair, $\mu(H^+) + \mu(e^-)$, is equal to the half of the chemical potential of one gaseous hydrogen, $1/2\mu(H_2)$, at U = 0 V *vs* SHE at pH = 0. The G was calculated by the following formula:

$$G=E + H(T) -TS$$

where E, H(T) and S are the electronic free energy, enthalpy and entropy of model at T = 298.15 K, respectively.

The highest reaction energy of elemental steps was used as the energy barrier in each pathway. Considering the charge balance of model, in the adsorption of NO_3^-, one proton was simultaneously adsorbed, which was equal to the adsorption of one HNO_3. Besides, in the reduction of NO_3^-, one proton would also directly bind with the adsorbed NO_3^- and reduce it into one adsorbed HNO_3 according to SHE models. Actually, the present adsorption step of HNO_3 consists of one NO_3^--adsorption step and one reduction step, which can simultaneously maintain the charge balance and the following reduction step.

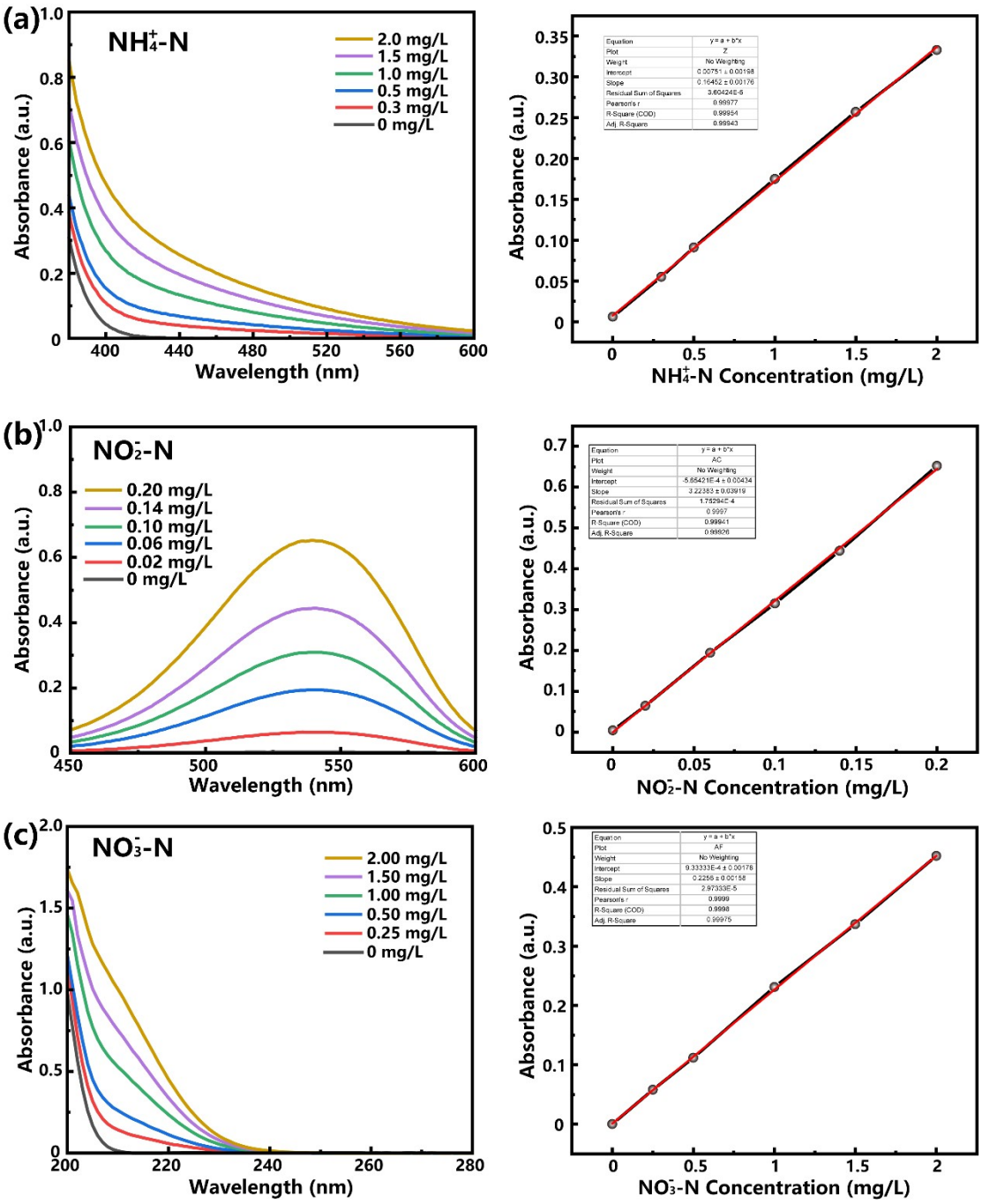

Figure S1. The UV-Vis absorption spectra in different concentration of (a) NH_4^+, (b) NO_2^-, (c) NO_3^- and the corresponding standard curve.

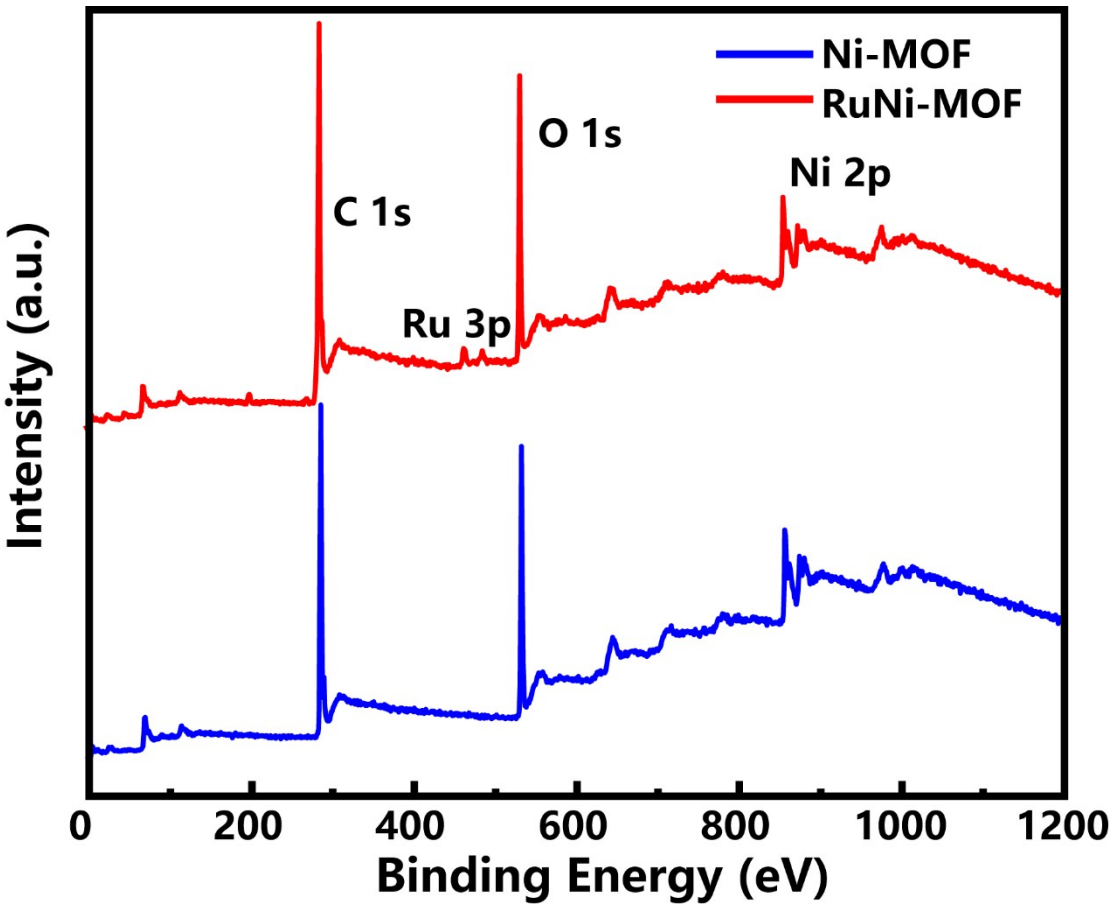

Figure S2. XPS pattern of Ni-MOF and RuNi-MOF.

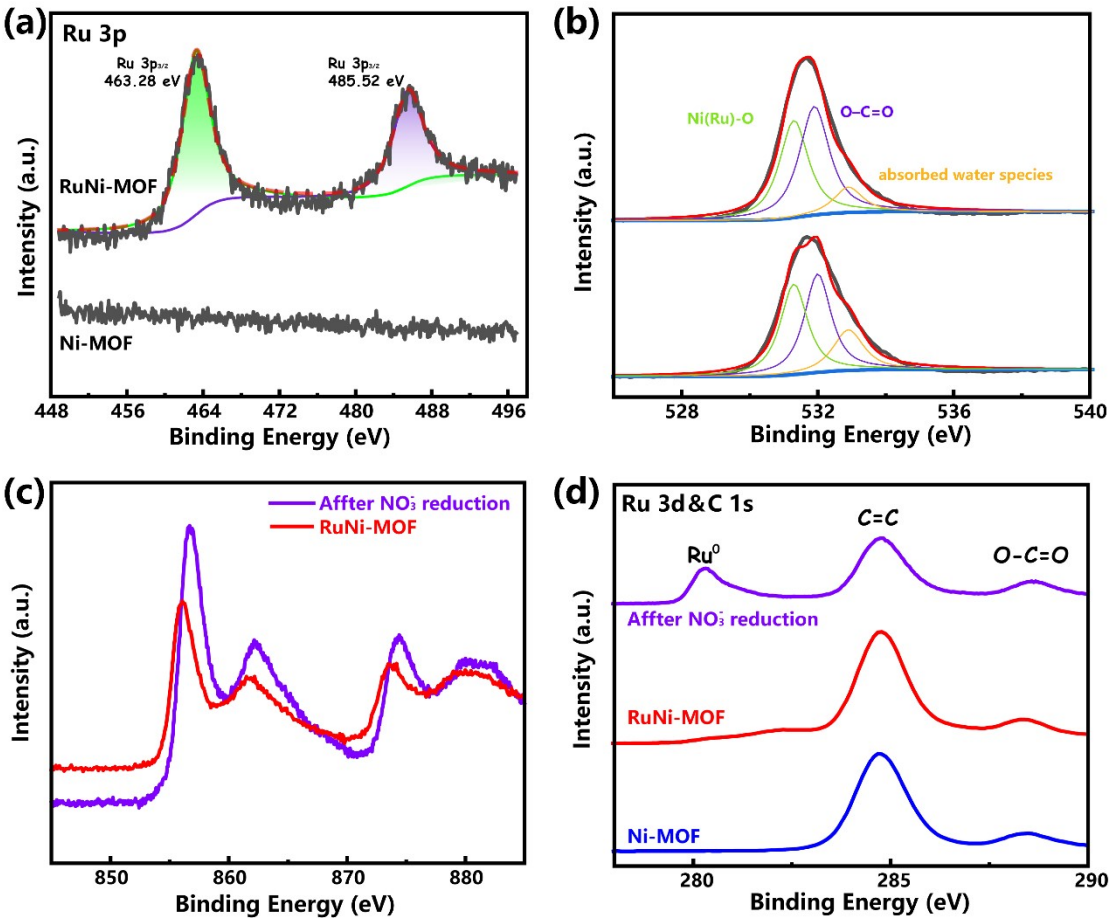

Figure S3. (a-b) Ru 3*p* and O 1*s* spectra of RuNi-MOF. (c-d) XPS spectra of Ni 2*p* and Ru 3*d* for RuNi-MOF catalysts before and after NO_3^- activation.

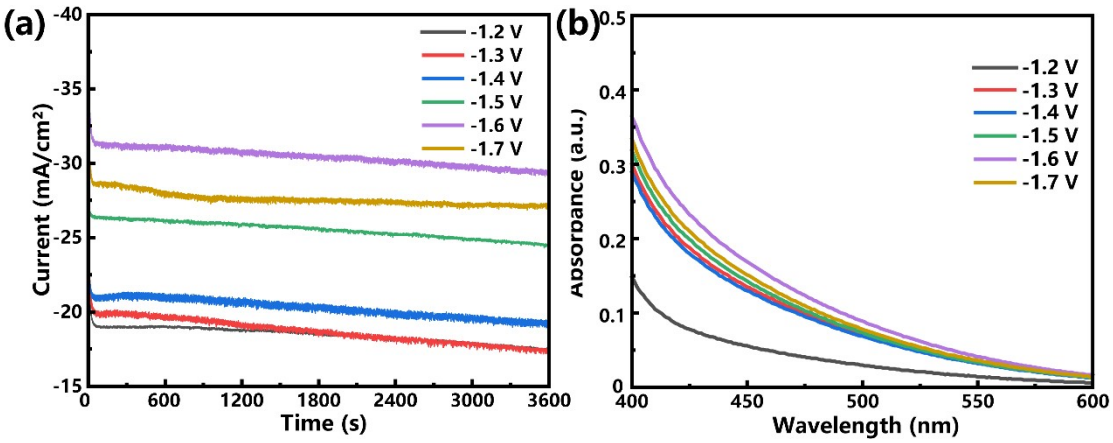

Figure S4. Chronoamperometric curves (a) and UV-vis absorption spectra (b) of the RuNi-MOF at various potentials in 50 mg/L NO_3^--N and 0.1 M $NaSO_4$ electrolytes.

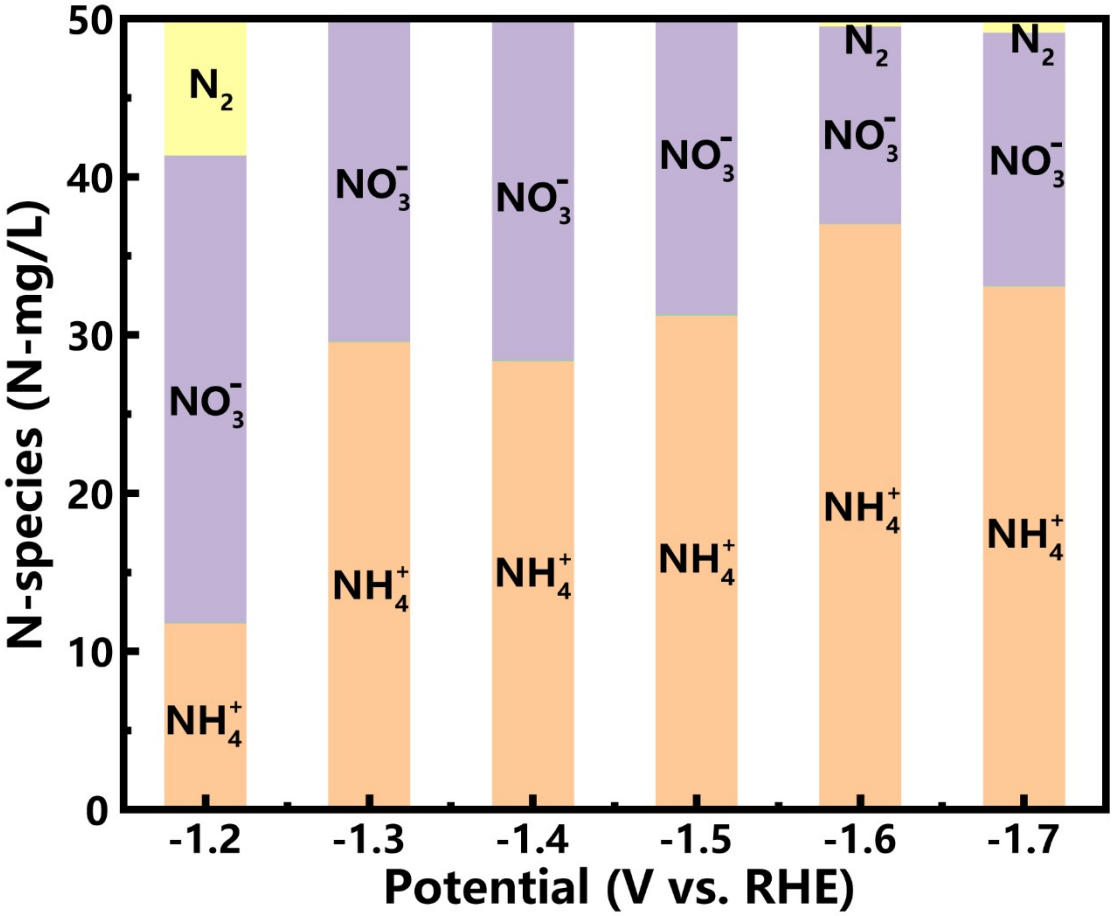

Figure S5. The mass balance of N-species at various potentials in 50 mg/L NO_3^--N and 0.1 M $NaSO_4$ electrolytes over the RuNi-MOF.

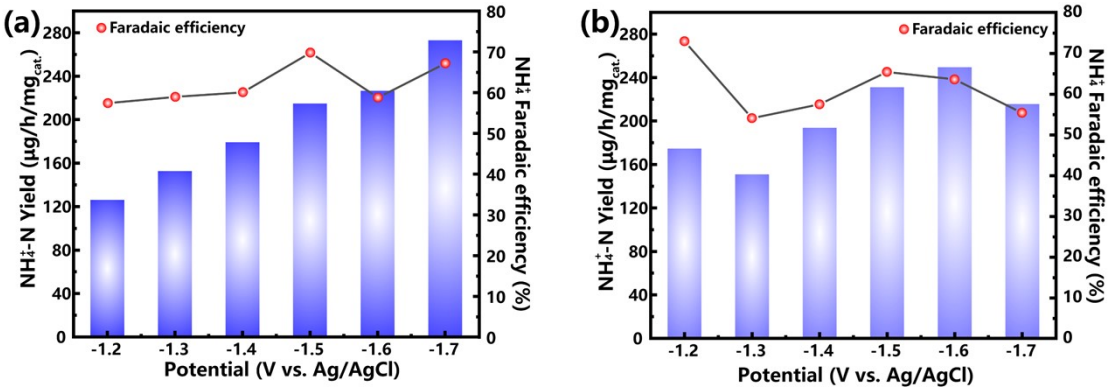

Figure S6. Potential-dependent NH_4^+ yield and Faradaic efficiency over RuNi-MOF at various potentials in 0.1 M $NaSO_4$ electrolytes containing 100 mg/L (a) or 200 mg/L (b) NO_3^--N.

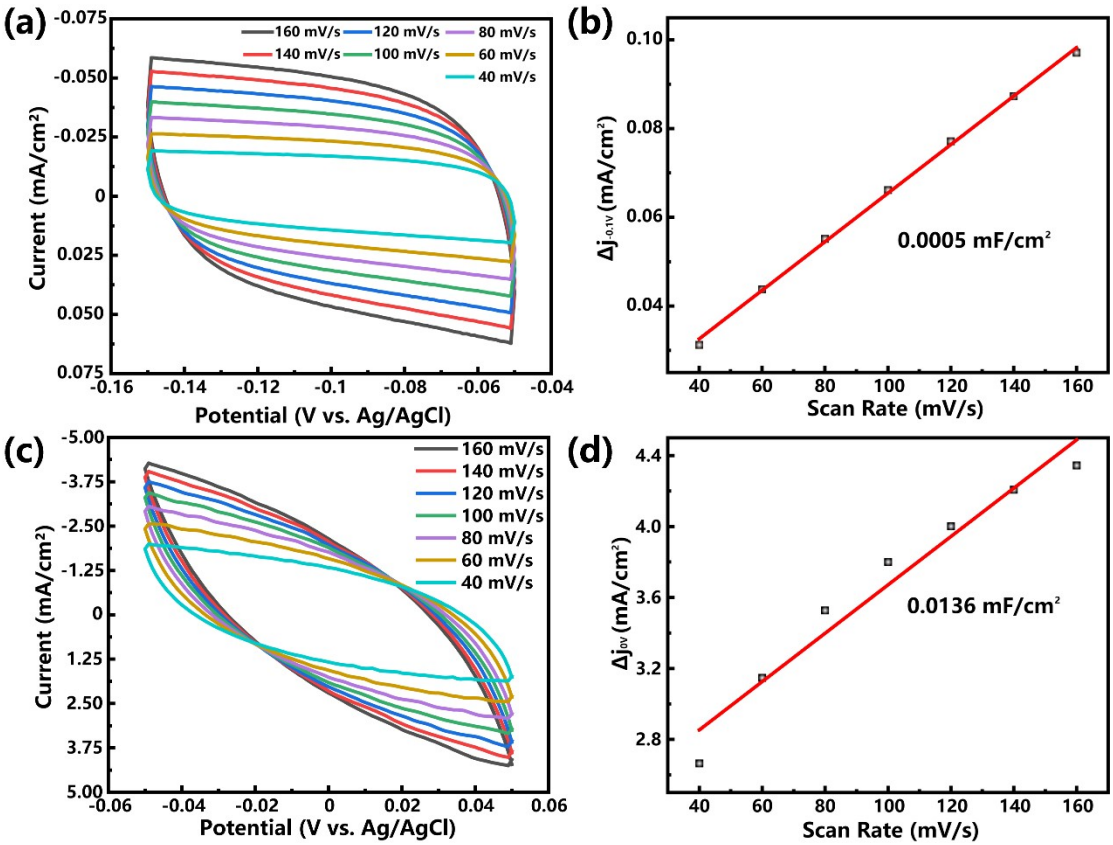

Figure S7. Cyclic voltammograms (CV) for (a) Ni-MOF and (c) RuNi-MOF at different scan rates from 20 to 160 mV/s, respectively. Double-layer capacitances (C_{dl}) calculated by the differences in current density as a linear function of scan rates of (b) Ni-MOF and (d) RuNi-MOF.

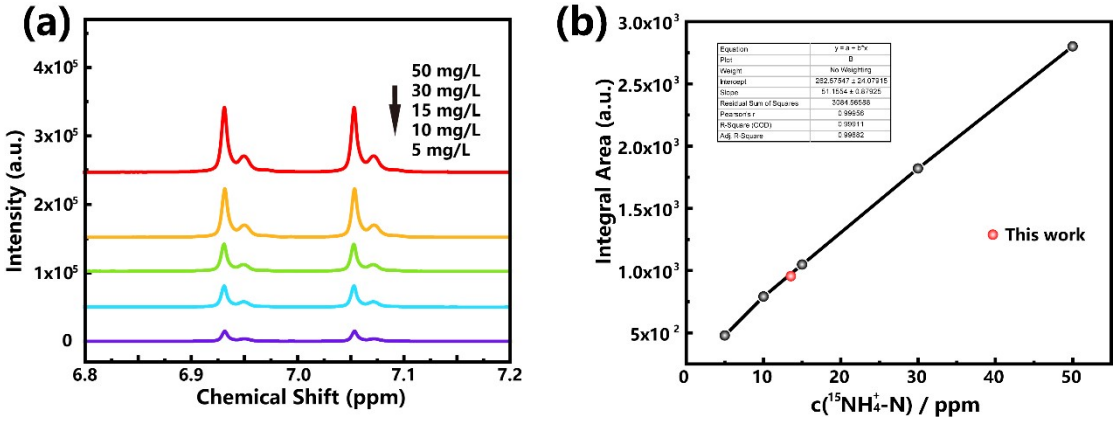

Figure S8. (a) ^{1}H NMR spectra of $^{15}NH_4^+$-^{15}N with different concentrations. (b) The standard curve of integral area ($^{15}NH_4^+$-^{15}N) against $^{15}NH_4^+$-^{15}N concentration.

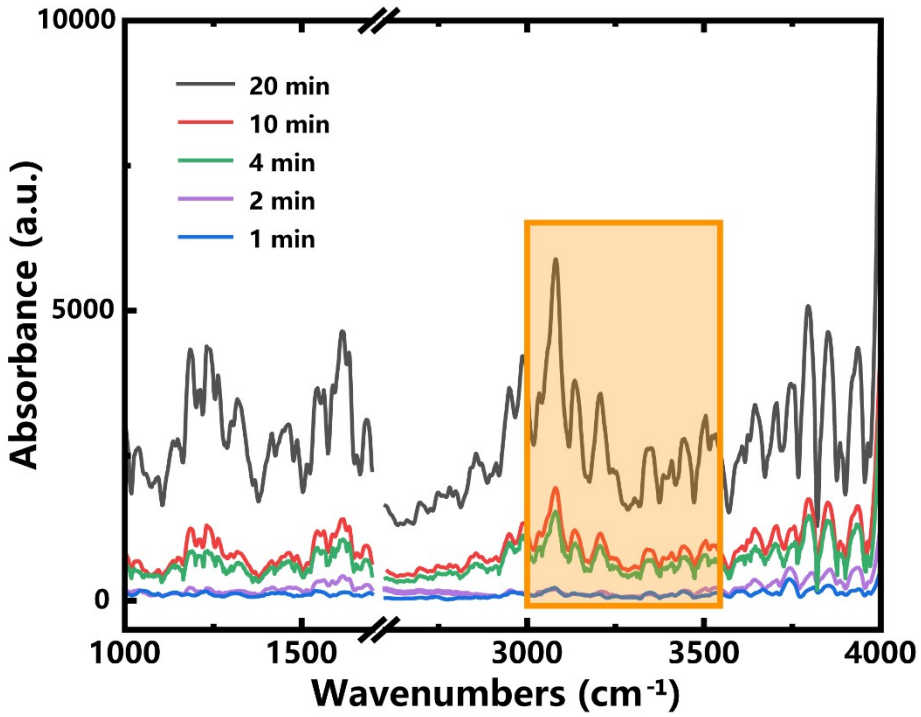

Figure S9. FT-IR spectroscopy measurements varying with time for RuNi-MOF.

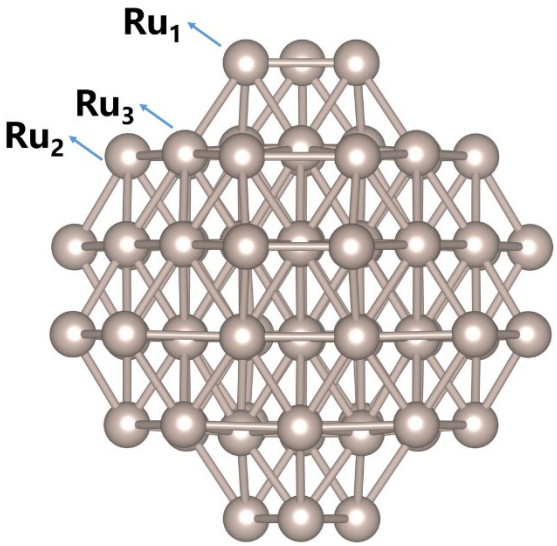

Figure S10. Ru nanoparticle displaying three different Ru sites: Five-coordinated Ru_1 site, six-coordinated Ru_2 site and eight-coordinated Ru_3 site.

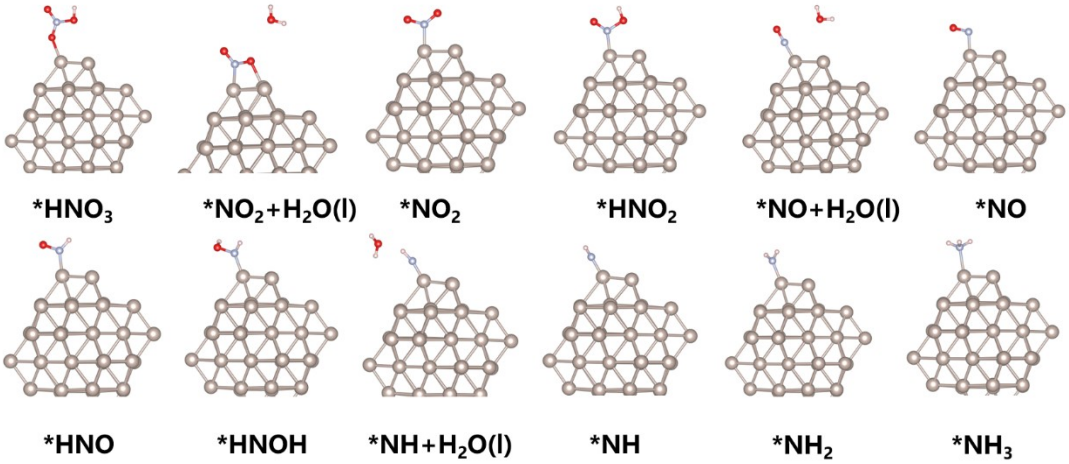

Figure S11. The reaction pathways of NO_3^- to NH_3 on Ru_1 sites.

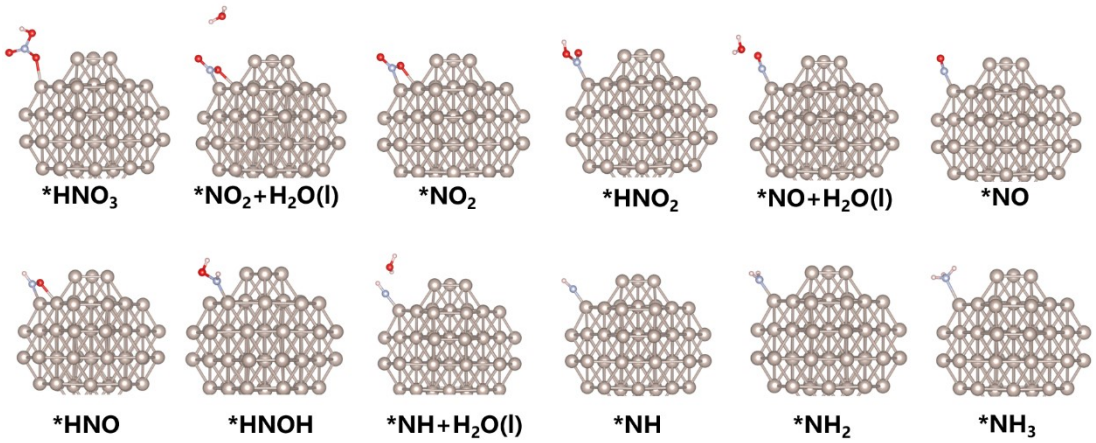

Figure S12. The reaction pathways of NO_3^- to NH_3 on Ru_2 sites.

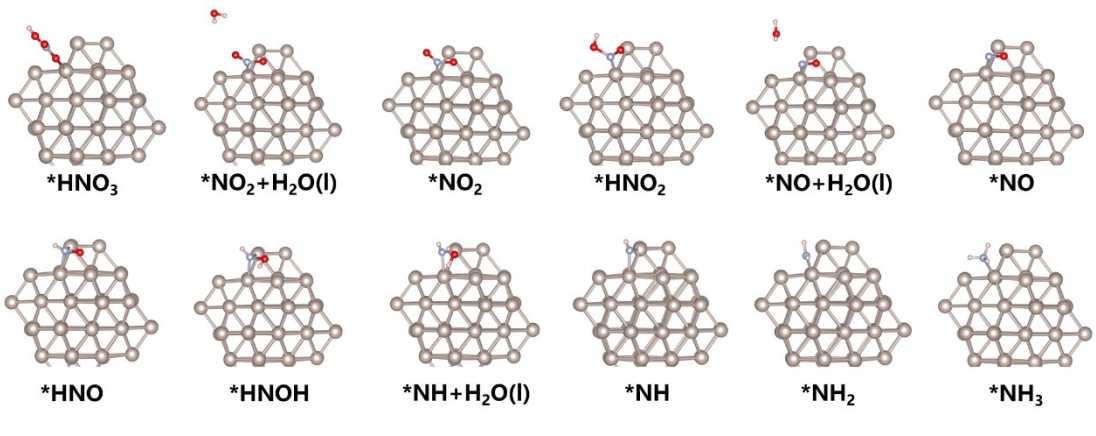

Figure S13. The reaction pathways of NO_3^- to NH_3 on Ru_3 sites.

Table 1. Comparison of performance of RuNi-MOF with reported catalysts by electrocatalytic NO_3^- reduction.

Catalyst	Electrolyte	NH_3 partial current	FE (%)	NO_3^--to-NH_3 selectivity (%)	Overpotential	Reference
RuNi-MOF	50 ppm NO_3^--N + 0.1 M $NaSO_4$	31.43 mA cm^{-2}	55.9	100		This work
	100 ppm NO_3^--N+0.1 M $NaSO_4$	31.45 mA cm^{-2}	58.8	100	-1.6 V vs. Ag/AgCl	
	200 ppm NO_3^--N+0.1 M $NaSO_4$	30.575 mA cm^{-2}	63.6%	100		
Fe SAC	0.5 M KNO_3/0.1 M KSO_4	98.6 mA cm^{-2}	74.9%	69	-0.66 V vs. RHE	2
TiO_{2-x}/Ti foil	50 ppm NO_3^--N+0.5 M $NaSO_4$	< 10 mA cm^{-2}	85	87.1	-1.6 V vs SCE	3
Cu/Cu_2O NWAs	200 ppm NO_3^--N+0.5 M $NaSO_4$	100 mA cm^{-2}	95.8	81.2	-0.85 V vs. RHE	4
Ni-Fe^0@ Fe_3O_4	50 ppm NO_3^- +10 mM NaCl	5 mA cm^{-2}	-	10.4	-1.4 V	5
Cu-incorporated PTCDA	0.1 mM PBS + 36 mM NO_3^-	-11.04 mA cm^{-2}	85.9	-	-0.4 V vs. RHE	6
OD-Co	1 M KOH	565.26 mA cm^{-2}	92.4	-	-0.8 V vs. RHE	7

Pd-Cu/SS	0.01 M $NaClO_4$ + 0.6 mM $NaNO_3$	-	-	6	-0.3 V vs. SCE	8
Cu nanosheets	0.1 M KOH + 10 mM KNO_3	-	99.7	-	-0.15 V vs. RHE	9

Table 2. All the enthalpy, ZPE, S values used for the mechanism studies.

*HNO_3	Ru_1	Ru_2	Ru_3
Zero-point energy E_ZPE:	15.601 kcal/mol	15.550 kcal/mol	15.693 kcal/mol
	0.676508 eV	0.674314 eV	0.680532 eV
Thermal correction to U(T):	18.767 kcal/mol	18.333 kcal/mol	18.437 kcal/mol
	0.813825 eV	0.794980 eV	0.799512 eV
Thermal correction to H(T):	18.767 kcal/mol	18.333 kcal/mol	18.437 kcal/mol
	0.813825 eV	0.794980 eV	0.799512 eV
Thermal correction to G(T):	12.797 kcal/mol	12.883 kcal/mol	12.974 kcal/mol
	0.554932 eV	0.558667 eV	0.562619 eV
Entropy S:	83.781 J/(mol*K)	76.474 J/(mol*K)	76.662 J/(mol*K)
	0.000868 eV/K	0.000793 eV/K	0.000795 eV/K
Electronic free energy:	-482.63 eV	-482.48 eV	-482.20 eV
*NO_2+H_2O	Ru_1	Ru_2	Ru_3
Zero-point energy E_ZPE:	19.317 kcal/mol	19.748 kcal/mol	19.247 kcal/mol
	0.837650 eV	0.856335 eV	0.834621 eV
Thermal correction to U(T):	22.076 kcal/mol	23.237 kcal/mol	21.963 kcal/mol
	0.957309 eV	1.007674 eV	0.952396 eV
Thermal correction to H(T):	22.076 kcal/mol	23.237 kcal/mol	21.963 kcal/mol
	0.957309 eV	1.007674 eV	0.952396 eV
Thermal correction to G(T):	16.943 kcal/mol	16.614 kcal/mol	17.086 kcal/mol
	0.734721 eV	0.720454 eV	0.740930 eV
Entropy S:	72.032 J/(mol*K)	92.948 J/(mol*K)	68.433 J/(mol*K)
	0.000747 eV/K	0.000963 eV/K	0.000709 eV/K
Electronic free energy:	-488.69 eV	-488.96 eV	-488.83 eV
*NO_2	Ru_1	Ru_2	Ru_3
Zero-point energy E_ZPE:	6.304 kcal/mol	5.582 kcal/mol	5.890 kcal/mol
	0.273354 eV	0.242052 eV	0.255407 eV
Thermal correction to U(T):	8.164 kcal/mol	6.514 kcal/mol	8.225 kcal/mol
	0.354007 eV	0.282493 eV	0.356659 eV
Thermal correction to H(T):	8.164 kcal/mol	6.514 kcal/mol	8.225 kcal/mol
	0.354007 eV	0.282493 eV	0.356659 eV
Thermal correction to G(T):	4.594 kcal/mol	5.024 kcal/mol	3.332 kcal/mol
	0.199222 eV	0.217865 eV	0.144496 eV
Entropy S:	50.090 J/(mol*K)	20.914 J/(mol*K)	68.659 J/(mol*K)
	0.000519 eV/K	0.000217 eV/K	0.000712 eV/K
Electronic free energy:	-474.56 eV	-474.95 eV	-474.76 eV
*HNO_2	Ru_1	Ru_2	Ru_3
Zero-point energy E_ZPE:	12.485 kcal/mol	12.469 kcal/mol	12.423 kcal/mol
	0.541380 eV	0.540713 eV	0.538726 eV
Thermal correction to U(T):	14.585 kcal/mol	14.131 kcal/mol	14.565 kcal/mol
	0.632449 eV	0.612787 eV	0.631591 eV
Thermal correction to H(T):	14.585 kcal/mol	14.131 kcal/mol	14.565 kcal/mol
	0.632449 eV	0.612787 eV	0.631591 eV

Thermal correction to G(T):	10.869 kcal/mol	11.135 kcal/mol	10.348 kcal/mol
	0.471342 eV	0.482855 eV	0.448748 eV
Entropy S:	52.136 J/(mol*K)	42.048 J/(mol*K)	59.170 J/(mol*K)
	0.000540 eV/K	0.000436 eV/K	0.000613 eV/K
Electronic free energy:	-478.02 eV	-478.22 eV	-477.85 eV
*NO+H_2O	Ru_1	Ru_2	Ru_3
Zero-point energy E_ZPE:	17.498 kcal/mol	17.938 kcal/mol	17.014 kcal/mol
	0.758790 eV	0.777868 eV	0.737804 eV
Thermal correction to U(T):	20.583 kcal/mol	21.808 kcal/mol	20.007 kcal/mol
	0.892554 eV	0.945698 eV	0.867593 eV
Thermal correction to H(T):	20.583 kcal/mol	21.808 kcal/mol	20.007 kcal/mol
	0.892554 eV	0.945698 eV	0.867593 eV
Thermal correction to G(T):	14.578 kcal/mol	14.127 kcal/mol	13.774 kcal/mol
	0.632178 eV	0.612613 eV	0.597288 eV
Entropy S:	84.261 J/(mol*K)	107.791 J/(mol*K)	87.474 J/(mol*K)
	0.000873 eV/K	0.001117 eV/K	0.000907 eV/K
Electronic free energy:	-483.57 eV	-483.40 eV	-483.32 eV
*NO	Ru_1	Ru_2	Ru_3
Zero-point energy E_ZPE:	3.287 kcal/mol	4.311 kcal/mol	4.002 kcal/mol
	0.142558 eV	0.186959 eV	0.173533 eV
Thermal correction to U(T):	4.722 kcal/mol	5.789 kcal/mol	5.279 kcal/mol
	0.204747 eV	0.251052 eV	0.228916 eV
Thermal correction to H(T):	4.722 kcal/mol	5.789 kcal/mol	5.279 kcal/mol
	0.204747 eV	0.251052 eV	0.228916 eV
Thermal correction to G(T):	1.812 kcal/mol	3.052 kcal/mol	3.101 kcal/mol
	0.078558 eV	0.132340 eV	0.134469 eV
Entropy S:	40.836 J/(mol*K)	38.417 J/(mol*K)	30.564 J/(mol*K)
	0.000423 eV/K	0.000398 eV/K	0.000317 eV/K
Electronic free energy:	-468.75 eV	-469.62 eV	-469.45 eV
*HNO	Ru_1	Ru_2	Ru_3
Zero-point energy E_ZPE:	10.399 kcal/mol	10.662 kcal/mol	11.104 kcal/mol
	0.450941 eV	0.462347 eV	0.481510 eV
Thermal correction to U(T):	12.337 kcal/mol	12.255 kcal/mol	12.385 kcal/mol
	0.534991 eV	0.531407 eV	0.537055 eV
Thermal correction to H(T):	12.337 kcal/mol	12.255 kcal/mol	12.385 kcal/mol
	0.534991 eV	0.531407 eV	0.537055 eV
Thermal correction to G(T):	8.523 kcal/mol	9.498 kcal/mol	10.342 kcal/mol
	0.369605 eV	0.411864 eV	0.448485 eV
Entropy S:	53.521 J/(mol*K)	38.686 J/(mol*K)	28.662 J/(mol*K)
	0.000555 eV/K	0.000401 eV/K	0.000297 eV/K
Electronic free energy:	-472.33 eV	-473.24 eV	-473.27 eV
*HNOH	Ru_1	Ru_2	Ru_3
Zero-point energy E_ZPE:	16.120 kcal/mol	17.055 kcal/mol	15.647 kcal/mol
	0.699022 eV	0.739575 eV	0.678499 eV

Thermal correction to U(T):	17.846 kcal/mol	19.198 kcal/mol	17.621 kcal/mol
	0.773863 eV	0.832486 eV	0.764108 eV
Thermal correction to H(T):	17.846 kcal/mol	19.198 kcal/mol	17.621 kcal/mol
	0.773863 eV	0.832486 eV	0.764108 eV
Thermal correction to G(T):	14.475 kcal/mol	15.363 kcal/mol	13.861 kcal/mol
	0.627696 eV	0.666206 eV	0.601088 eV
Entropy S:	47.302 J/(mol*K)	53.810 J/(mol*K)	52.755 J/(mol*K)
	0.000490 eV/K	0.000558 eV/K	0.000547 eV/K
Electronic free energy:	-476.07 eV	-476.13 eV	-476.24 eV
*NH+H_2O	Ru_1	Ru_2	Ru_3
Zero-point energy E_ZPE:	21.322 kcal/mol	20.175 kcal/mol	21.201 kcal/mol
	0.924620 eV	0.874883 eV	0.919350 eV
Thermal correction to U(T):	24.078 kcal/mol	22.686 kcal/mol	24.192 kcal/mol
	1.044118 eV	0.983768 eV	1.049060 eV
Thermal correction to H(T):	24.078 kcal/mol	22.686 kcal/mol	24.192 kcal/mol
	1.044118 eV	0.983768 eV	1.049060 eV
Thermal correction to G(T):	18.767 kcal/mol	17.943 kcal/mol	18.239 kcal/mol
	0.813821 eV	0.778093 eV	0.790913 eV
Entropy S:	74.527 J/(mol*K)	66.559 J/(mol*K)	83.540 J/(mol*K)
	0.000772 eV/K	0.000690 eV/K	0.000866 eV/K
Electronic free energy:	-481.14 eV	-480.96 eV	-481.71 eV
*NH	Ru_1	Ru_2	Ru_3
Zero-point energy E_ZPE:	7.264 kcal/mol	7.123 kcal/mol	7.615 kcal/mol
	0.314992 eV	0.308863 eV	0.330201 eV
Thermal correction to U(T):	8.520 kcal/mol	8.500 kcal/mol	8.739 kcal/mol
	0.369457 eV	0.368587 eV	0.378938 eV
Thermal correction to H(T):	8.520 kcal/mol	8.500 kcal/mol	8.739 kcal/mol
	0.369457 eV	0.368587 eV	0.378938 eV
Thermal correction to G(T):	6.285 kcal/mol	5.983 kcal/mol	6.851 kcal/mol
	0.272522 eV	0.259453 eV	0.297066 eV
Entropy S:	31.369 J/(mol*K)	35.317 J/(mol*K)	26.495 J/(mol*K)
	0.000325 eV/K	0.000366 eV/K	0.000275 eV/K
Electronic free energy:	-467.30 eV	-467.15 eV	-467.61 eV
*NH_2	Ru_1	Ru_2	Ru_3
Zero-point energy E_ZPE:	14.421 kcal/mol	14.703 kcal/mol	14.414 kcal/mol
	0.625335 eV	0.637566 eV	0.625037 eV
Thermal correction to U(T):	16.075 kcal/mol	16.189 kcal/mol	16.093 kcal/mol
	0.697092 eV	0.702026 eV	0.697842 eV
Thermal correction to H(T):	16.075 kcal/mol	16.189 kcal/mol	16.093 kcal/mol
	0.697092 eV	0.702026 eV	0.697842 eV
Thermal correction to G(T):	12.967 kcal/mol	13.518 kcal/mol	12.880 kcal/mol
	0.562285 eV	0.586216 eV	0.558518 eV
Entropy S:	43.625 J/(mol*K)	37.478 J/(mol*K)	45.087 J/(mol*K)
	0.000452 eV/K	0.000388 eV/K	0.000467 eV/K

Electronic free energy:	-471.48 eV	-471.43 eV	-470.83 eV
*NH_3	Ru_1	Ru_2	Ru_3
Zero-point energy E_ZPE:	22.920 kcal/mol	23.053 kcal/mol	22.976 kcal/mol
	0.993899 eV	0.999693 eV	0.996333 eV
Thermal correction to U(T):	24.721 kcal/mol	24.818 kcal/mol	24.694 kcal/mol
	1.072001 eV	1.076189 eV	1.070849 eV
Thermal correction to H(T):	24.721 kcal/mol	24.818 kcal/mol	24.694 kcal/mol
	1.072001 eV	1.076189 eV	1.070849 eV
Thermal correction to G(T):	21.125 kcal/mol	21.520 kcal/mol	21.592 kcal/mol
	0.916059 eV	0.933212 eV	0.936316 eV
Entropy S:	50.465 J/(mol*K)	46.269 J/(mol*K)	43.537 J/(mol*K)
	0.000523 eV/K	0.000480 eV/K	0.000451 eV/K
Electronic free energy:	-475.30 eV	-475.32 eV	-475.02 eV

Supplementary references

1. Nørskov J. K. et al. Origin of the overpotential for oxygen reduction at a fuel-cell cathode. *J Phys Chem B* 2004, 108, 17886-17892.
2. Wu, Z. et al. Electrochemical ammonia synthesis via nitrate reduction on Fe single atom catalyst. *Nat. Commun.* 2021, 12, 2870.
3. Jia, R. et al. Boosting selective nitrate electroreduction to ammonium by constructing oxygen vacancies in TiO_2. *ACS Catal.* 2020, 10, 3533-3540.
4. Wang, Y. et al. Unveiling the activity origin of a copper-based electrocatalyst for selective nitrate reduction to ammonia. *Angew. Chem. Int. Ed.* 2020, 59, 5350-5354.
5. Yin, D. et al. In situ growth of copper/reduced graphene oxide on graphite surfaces for the electrocatalytic reduction of nitrate. *Electrochim. Acta* 2019, 324, 134846.
6. Chen, G.-F. et al. Electrochemical reduction of nitrate to ammonia via direct eight-electron transfer using a copper-molecular solid catalyst. *Nat. Energy* 2020, 5, 605-613.
7. Kani, N. C. et al. Solar-driven electrochemical synthesis of ammonia using nitrate with 11% solar-to-fuel efficiency at ambient conditions. Energy & Environ. Sci. 2021. DOI: 10.1039/d1ee01879e.
8. Su, J. F. et al. The electrochemical reduction of nitrate over micro-architectured metal electrodes with stainless steel scaffold. *Appl. Catal., B* 2016*,* 180, 199-209.
9. Fu, X. et al. Alternative route for electrochemical ammonia synthesis by reduction of nitrate on copper nanosheets. *Appl. Mater. Today* 2020, 19, 100620.